Advent of complex flows in epithelial tissues

Pilhwa Lee and Charles Wolgemuth

Phys. Rev. E **83**, 061920 — Published 27 June 2011

DOI: 10.1103/PhysRevE.83.061920

Advent of complex flows in epithelial tissues

Pilhwa Lee and Charles Wolgemuth*

Department of Cell Biology and Center for Cell Analysis and Modeling,

University of Connecticut Health Center,

263 Farmington Avenue, Farmington, CT 06030-6406

Abstract

The collective migration of cells in tissue pervades many important biological processes, such as wound healing, organism development, and cancer metastasis. Recent experiments on wound healing show that the collective migratory behavior of cells can be quite complex, including transient vortices and long-range correlations. Here, we explore cellular flows in epithelial tissues using a model that considers the force distribution and polarity of a single cell along with cell-cell adhesion. We show that the dipole nature of a crawling cell's force distribution destabilizes steady cellular motion. We determine the values of the physical parameters that are necessary to produce these complex motions and use numerical simulation to verify the linear analysis and to demonstrate the complex flows. We find that the tendency for cells to align is the dominant physical parameter that determines the stability of steady flows in the epithelium.

PACS numbers: 87.18.Gh,87.19.R-,87.18.Vf

* cwolgemuth@uchc.edu

I. INTRODUCTION

When an animal's skin is cut, a salient feature of the wound healing process involves collective cell migration. Within hours after injury, epithelial cells at the periphery of the wound crawl over the wounded region in order to reform a monolayer of epithelial cells, a process known as *re-epithelialization* [1]. A standard experimental method for investigating this process is the wound healing assay, where a continuous monolayer of epithelial cells is "wounded" by scraping away or removing a swath of cells. The mechanism underlying re-epithelialization was originally presumed to involve chemical signaling within the monolayer that identified the wounded region and marshalled cells to crawl into the void. Experiments over the last ten years, though, suggest a more mechanical viewpoint. For example, deactivating a row of cells at the wound periphery does not inhibit wound closure [2], cells away from the wound are motile [3], and long-range correlations and complex flow patterns that include vortices are observed in the cellular velocity field [4, 5].

Based on these observations, a model was proposed recently to describe the relelvant physical mechanisms that may drive re-epithelialization [6]. This model assumes that the migratory behavior of cells in tissues can be described largely by a few basic biophysical processes that are present in motile tissue cells. Specifically, the model proposes that the fundamental driving force behind the collective migration that accompanies wound healing is the active contractile stress generated within polarized epithelial cells coupled with cell-cell adhesion.

II. DESCRIPTION OF THE MODEL

Most crawling eukaryotic cells drive motility in a similar fashion. Polymerization at the leading edge pushes out the front of the cell, while contractile forces inside the cell pull the rear of the cell forward. These cellular motions are driven by the motion of the internal actin cytoskeleton. Proteins, such as integrin, connect the cell's actin cytoskeleton to the substrate or extracellular matrix [7], which allows these actin flows to exert traction stresses onto the substrate [8–10]. It is likely that the contractile forces are the dominant forces that control how a cell interacts with its surroundings, since cells plated on a semi-rigid substrate pull forward at the rear of the cell and backward at the front of the cell [8, 9, 11, 12]. In

other words, individual cells produce dipole-distributed stresses (Fig. 1). These dipole-distributed stresses lead to a net thrust force $\mathbf{F}$ that propels the cell at roughly constant velocity $V_0\boldsymbol{d}$ when other cells are not present, where $\boldsymbol{d}$ is a unit vector that defines the polarization direction of the cell (Fig. 1). Isolated Madin-Darby canine kidney (MDCK) cells, which are often used in wound healing assays, are typically around 20 μm in diameter and move at speeds of about 10 μm/hr [13]. The turnover rate of integrin is on order of minutes [14], which is fast compared to the crawling speed fof the cell. This allows us to treat the interaction between the cytoskeleton and the substrate as a resistive drag force that is proportional to the velocity [15, 16]. The propulsive force is, therefore, $\mathbf{F} = \zeta V_0\boldsymbol{d}$, where ζ is a drag coefficient (Fig. 1).

Epithelial cells can also adhere to one another through cadherin junctions. Therefore, when motile epithelial cells are in contact with one another, the contractile forces within the cell are transmitted to its neighbors. The cadherin molecules that form the adhesions turnover on time scales of less than an hour [17], whereas the bulk motions that occur during wound healing take tens of hours to complete. Therefore, these adhesions behave more like viscoelastic connections than rigid adhesions.

A simple mean-field description of an epithelium can be constructed by considering small volume elements that are larger than the size of a cell but small compared to the size of the tissue. On these length scales, the adhesive forces that act between neighboring cells can be described by a stress tensor, $\boldsymbol{\sigma}_c$. In addition to this stress, there is also the active dipole stress that is created by a single cell, which is defined by the tensor $\boldsymbol{\sigma}_d$. If the cell is oriented along a direction $\hat{\mathbf{d}}$, then the simplest form for the dipole-distributed stress is $\boldsymbol{\sigma}_d = f_0 b \hat{\mathbf{d}}\hat{\mathbf{d}}$, where f_0 is the magnitude of the force that the cell exerts against the substrate and b is the length of the cell. In addition to these two stresses, a crawling cell also exerts the propulsive force against the substrate that is mentioned above, and there is a resistive force exerted on the cell when it moves with respect to the substrate. In the presence of other cells, a single cell does not move at velocity $V_0\hat{\mathbf{d}}$ because the interaction between neighboring cells change the total force that is exerted on the cell. The cell therefore crawls at velocity $\boldsymbol{v}$, and the resistive force is $\zeta\boldsymbol{v}$. Force balance for a unit volume in the epithelial tissue is then governed by

$$\nabla \cdot \boldsymbol{\sigma}_c - \nabla \cdot (b\boldsymbol{d}\boldsymbol{d}) + \zeta V_0 \boldsymbol{d} - \zeta \boldsymbol{v} = 0 \ . \tag{1}$$

As mentioned previously, turnover of the cadherin molecules in the cell adhesion junctions leads to viscoelastic behavior. On timescales shorter than the cadherin turnover time, τ, the molecules in the adhesion are firmly anchored and neighboring cells that move with respect to each other experience elastic restoring forces. On timescales longer than τ, there can be sliding of the cells with respect to each other, and the response is more like a viscous fluid with viscosity η [6, 15, 16, 18]. In addition, cells in an epithelial monolayer overlap with one another [3]. Therefore, when one treats the monolayer as a two-dimensional object, the total area occupied by the layer can change. However, we expect that larger resistive forces are encountered when the cell motions act to change the total density rather than when they result in pure shear deformations. We, therefore, define a *volumetric* viscosity λ that describes the resistive forces that arise due to motions that change the density. The simplest model that contains these features is the Maxwell fluid model, and it can be shown that chemical reaction kinetics with spring like adhesion molecules satisfy this type of equation in the limit where the force is small compared to the maximum force that the molecules can withstand [6]. The cell-cell adhesion stress then obeys

$$\boldsymbol{\sigma}_c + \tau \frac{\partial \boldsymbol{\sigma}_c}{\partial t} = \frac{\eta}{2}(\nabla \boldsymbol{v} + (\nabla \boldsymbol{v})^T) + (\lambda - \frac{\eta}{2})(\nabla \cdot \boldsymbol{v})\mathbf{I} \ , \tag{2}$$

where $\mathbf{I}$ is the identity matrix.

Finally, we need to account for the dynamics of the cell orientation. We assume that there is a tendency for nearby cells to align. Presumably this interaction may be driven by the cell elasticity. If a cell is slightly elongated in its direction of motion, then splay between neighboring cells will produce an elastic restoring force. This interaction will behave like the splay force in a nematic liquid crystal. We define a single Franck constant K to define the magnitude of the restoring force in terms of the splay. The orientation of the cells is also affected by local cellular motion, where vorticity in the cellular flow field will reorient the cells. Balancing the convective derivative with the reorientational effects of elasticity and vorticity, we get a nematic hydrodynamic-like equation for the dynamics of the orientation field:

$$\zeta_r \left(\frac{\partial \boldsymbol{d}}{\partial t} + \boldsymbol{v} \cdot \nabla \boldsymbol{d} - \frac{1}{2}(\nabla \times \boldsymbol{v}) \times \boldsymbol{d} \right) = K \nabla^2 \boldsymbol{d} \ , \tag{3}$$

where ζ_r is a rotational drag coefficient.

This system of equations was recently analyzed numerically and was shown to agree quantitatively with many of the observed features in wound healing assays [6]. In this

paper, we explore the linear stability of these equations, which should serve to provide a quantitative view of the parameter space and how the collective dynamics of cells in tissue can be regulated. Indeed, different cell lines are observed to behave quite differently [5], and this analysis may provide a useful measure for how these differences arise. It should also be noted that these equations are similar to the equations that have been used to describe the collective motion of self-propelled micro-organisms, which have been studied by several groups [19–22]. There are two primary differences between our equations and those used for swimming bacteria. First, it has been shown that the overall dynamics during wound healing are not srongly dependent on cell division. We therefore do not directly treat the density of the cells in our system. Second, the interactions between our cells are mediated by a viscoelastic stress, as opposed to a purely viscous fluid stress.

III. RESULTS

Linear Stability Analysis. It is useful to non-dimensionalize the system of equations using a characteristic tissue size L, a time scale L/V_0, and the thrust force ζV_0. There are then five non-dimensional parameters of the model:

$$\tilde{b} = \frac{bf_0}{\zeta V_0 L}, \quad \tilde{\eta} = \frac{\eta}{\zeta L^2}, \quad \tilde{\lambda} = \frac{\lambda}{\zeta L^2},$$
$$\tilde{K} = \frac{K}{\zeta_r L V_0}, \quad \tilde{\tau} = \frac{V_0 \tau}{L} \ . \tag{4}$$

The dimensionless velocity and stress are

$$\tilde{\boldsymbol{v}} = \frac{\boldsymbol{v}}{v_0}, \quad \tilde{\boldsymbol{\sigma}} = \frac{\boldsymbol{\sigma}_c}{\zeta V_0} \ . \tag{5}$$

To carry out the linear stability analysis, we consider a scenario that precedes some of the recent wound healing assay experiments. Silberzan and coworkers have developed a micro-patterned stencil that allows them to grow an epithelial monolayer inside a rectangular well [4]. The stencil can then be removed, and the cells crawl to fill in the newly vacated substrate. We consider a system such as this before the stencil is removed: an infinite swath of cells bounded on the top and bottom by rigid walls. We define the swath to be aligned with the x-axis and assume that the cells are also initially aligned with the x-axis. It is straightforward to show that if the cell alignment is uniformly directed along the x axis,

then the velocity of the cells is also along the x axis. We, therefore, consider perturbations to the steady flow solution:

$$\boldsymbol{d} = \boldsymbol{x} + \epsilon d_y \boldsymbol{y} \ , \tag{6}$$

$$\boldsymbol{v} = (1 + \epsilon v_x)\, \boldsymbol{x} + \epsilon v_y \boldsymbol{y} \ , \tag{7}$$

where $\epsilon << 1$ and we have not included an equation for $\boldsymbol{\sigma}$ as it is possible to remove $\boldsymbol{\sigma}$ from the equations using the divergence of Eq. 2.

Expanding the force balance equation (Eq. 1) and the orientational dynamics equation (Eq. 3) to first order in ϵ using Eqs. 6–7 leads to the following linearized equations:

$$\frac{\partial d_y}{\partial t} = -\frac{\partial d_y}{\partial x} + \frac{1}{2}(\frac{\partial v_y}{\partial x} - \frac{\partial v_x}{\partial y}) + K\nabla^2 d_y \ , \tag{8}$$

$$\begin{aligned}\tau\frac{\partial v_x}{\partial t} = {} & \eta\nabla^2 v_x - v_x + (\lambda - \frac{\eta}{2})(\frac{\partial^2 v_x}{\partial^2 x} + \frac{\partial^2 v_y}{\partial x \partial y}) \\ & -b\frac{\partial d_y}{\partial y} - \tau b\frac{\partial^2 d_y}{\partial t \partial y} \ ,\end{aligned} \tag{9}$$

$$\begin{aligned}\tau\frac{\partial v_y}{\partial t} = {} & \eta\nabla^2 v_y - v_y + (\lambda - \frac{\eta}{2})(\frac{\partial^2 v_x}{\partial x \partial y} + \frac{\partial^2 v_y}{\partial y^2}) \\ & -b\frac{\partial d_y}{\partial x} + d_y - \tau b\frac{\partial^2 d_y}{\partial t \partial x} + \tau\frac{\partial d_y}{\partial t} \ .\end{aligned} \tag{10}$$

In Eqs. 8-10, we have dropped the tildes from the non-dimensional parameters. We maintain this notation throughout the remainder of the paper.

We now look for solutions of the form $d_y = \hat{d}_y(\boldsymbol{k})e^{i(\boldsymbol{k}\cdot\boldsymbol{x} - \omega t)}$, where $\boldsymbol{k} = (k_x, k_y)$ is the wave vector and the corresponding frequency is $\omega = \gamma_R + i\gamma_I$. The real part of the frequency, γ_R, gives the oscillation frequency of the mode and the growth rate is γ_I. Similar equations are used for v_x and v_y. Substituting these expressions for d_y, v_x, and v_y into Eqs. 8–10, leads to a linear system of equations with determinant

$$\begin{vmatrix} K|k|^2 - i\omega + ik_x & \frac{1}{2}ik_y & -\frac{1}{2}ik_x \\ ibk_y(1 - i\tau\omega) & \Omega + \Lambda k_x^2 & \Lambda k_x k_y \\ (ibk_x - 1)(1 - i\tau\omega) & \Lambda k_x k_y & \Omega + \Lambda k_y^2 \end{vmatrix} \ , \tag{11}$$

with $\Omega = 1 - i\tau\omega + \eta|k|^2$ and $\Lambda = \lambda - \frac{\eta}{2}$. For non-trivial solutions the determinant is zero, which gives a cubic equation that sets ω in terms of the wavenumber $\boldsymbol{k}$ and the parameters τ, b, η, λ, and K.

Following [21], we define θ to be the angle between $\boldsymbol{k}$ and $\boldsymbol{x}$. In Fig. 2a, we plot the maximal growth rate as a function of the magnitude of the wave number and θ using reasonable parameter values for MDCK epithelial cells: $b = 0.1$; $\eta = 0.0025$; $K = 0.025$; and $\tau = 0.025$ [6]. The non-dimensionalization that is used to compute these parameters corresponds with a wound size $L \approx 200\mu$m, a crawling speed $V_0 = 10\mu$m/hr, and a drag coefficient $\zeta = 100$ pN$\cdot$hr/μm^3. For these parameters, we find that uniform motion of the cells is unstable, with a maximum growth rate when $k = 10.8$. This wavenumber corresponds to a wavelength of $\sim 120\mu$m, which is approximately equal to the velocity correlation length that is observed in experiments [4]. The growth rate is largest for perturbations along the x direction (Fig. 2a), therefore, we expect uniform crawling to initially break into a roll-type pattern at the onset of the instability. The temporal frequency increases roughly linearly with k.

In order to gain intuition for the physics that leads to complex flows in epithelial tissues, we determined the parameter regimes where uniform motion of the epithelium are stable (i.e., where the maximal growth rate is negative). In Fig. 2, we plot the bifurcation diagrams as a function of pairs of the dimensionless parameters. We find that the dimensionless dipole stress magnitude b and the viscoelastic time scale τ are destabilizing factors that drive the system to non-steady flow patterns, whereas the orientational Franck constant K is a stabilizing factor. Indeed, without a tendency to align, the uniform state is unconditionally unstable, as in the case of active suspensions [21]. This finding also agrees with the dimensional analysis arguments that were given in [22], which suggested that complex flows in bacterial systems involve a competition between the tendency to algin and convective instabilities. We also find that the cell-cell viscosity η does not strongly affect the stability of the uniform flow state. Fig. 2 also shows the magnitude of the dominant wavenumber, which gives an indication of the size of the vortices that would be observed in experiments. The Franck constant and the cell-cell viscosity both lead to longer length correlations in the cellular flow field, whereas the viscoelastic timescale decreases the correlation length.

Numerical simulations. In order to validate our linear analysis and to determine the overall large scale behavior of the system after onset, we simulated Eqs. 1–3, on a rectangular domain (200μm $\times$ 800μm). We used periodic boundary conditions on the left and right sides of the domain, and treated the top and bottom as rigid walls. On these walls, the normal component of the velocity was set to zero. In addition, we assumed no net torque on the

walls ($(\hat{\mathbf{n}}\cdot\nabla)\hat{\mathbf{d}} = 0$), and zero tangential force ($\hat{\mathbf{t}}\cdot\boldsymbol{\sigma}\cdot\hat{\mathbf{n}} = 0$), where $\hat{\mathbf{n}}$ is the normal to the wall and $\hat{\mathbf{t}}$ is the tangent. To numerically solve the equations we used a finite volume approach described in [23]. For any values of parameters that we used that fell in the stable regime, we observed steady migratory behavior along the x axis (Fig. 3a). It should be noted that this is idealized behavior that would not be noticed in an experiment, as the x extent is finite and prevents net constant displacements. For parameters in the unstable regime, cells initially migrate along the x direction, but after a while, perturbations adjacent to walls and then propogate in through the whole domain (Fig. 3b-d). The emerging vortices are transient, appearing and disapperaing in a seemingly random fashion.

IV. CONCLUSION

The results presented here show that the basic physics of eukaryotic cell motility are sufficient to drive complex collective motions in populations of cells that can adhere to one another. We find that for reasonable values of the model parameters (i.e., those corresponding to MDCK cell lines) that transient vortical flows are expected in these tissues and that the length scale of the dominant mode is comparable to what has been observed in experiments [4]. In addition, we have elucidated the role that the model parameters play in creating the complex flows and the dependence of the dominant wavelength on these parameters. Experiments that can alter these physical parameters, such as using substrates of varying stiffness or altering expression levels of proteins that influence actin dynamics, can be used to test these predictions. Because this model is based on the general physical behavior of crawling cells, we expect that this phenomenon is not only applicable to epithelial sheets, but may also be relevant for the collective migration of cells during organism development and cancer metastasis [24, 25]. An interesting question remains: Do these complex flows serve an important biological function?

ACKNOWLEDGMENTS

The research was supported by the NSF (DMS 0920279).

---

[1] T. Velnar, T. Bailey, and C. Smrkolj, J. Int. Med. Res. **37**, 1528 (2009).

[2] G. Fenteany, P. Janmey, and T. Stossel, Curr. Biol. **10**, 831 (2000).

[3] R. Farooqui and G. Fenteany, J. Cell Sci. **118**, 51 (2005).

[4] M. Poujade, E. Grasland-Mongrain, A. Hertzog, J. Jouanneau, P. Chavrier, B. Ladoux, A. Buguin, and P. Silberzan, Proc. Natl. Acad. Sci. USA **104**, 15988 (2007).

[5] L. Petitjean, M. Reffay, E. Grasland-Mongrain, M. Poujade, B. Ladoux, A. Buguin, and P. Silberzan, Biophys. J. **98**, 1790 (2010).

[6] P. Lee and C. Wolgemuth, PLoS Comput. Biol. **7**, e1002007 (2011).

[7] C. K. Choi, et al, Nat. Cell Biol. **10**, 1039 (2008).

[8] A. D. Doyle and J. Lee, Biotechniques **32**, 358 (2002).

[9] M. Dembo and Y.-L. Wang, Biophys. J. **76**, 2307 (1999).

[10] O. du Roure, et al, Proc. Natl. Acad. Sci. USA **102**, 2390 (2005).

[11] C.-M. L. D. B. Buxton, G. C. H. Chua, M. Dembo, R. S. Adelstein, and Y.-L. Wang, Mol. Biol. Cell **15**, 982 (2004).

[12] Y.-T. Shiu, S. Li, W. A. Marganski, S. Usami, M. A. Schwartz, Y.-L. Wang, M. Dembo, and S. Chien, Biophys. J. **86**, 2558 (2004).

[13] M. Boca, et al, Mol. Biol. Cell **18**, 4050 (2007).

[14] C. Cluzel, et al, J. Cell Biol., **171**, 383 (2005).

[15] S. Walcott and S. X. Sun, Proc. Natl. Acad. Sci. USA **107**, 7757 (2010).

[16] S. Leibler and D. A. Huse, J. Cell Biol. **121**, 1357 (1993).

[17] M. Lambert, O. Thoumine, J. Brevier, D. Choquet, D. Riveline, and R.-M. Mege, Exp. Cell Res. **313**, 4025 (2007).

[18] H. M. Lacker and C. S. Peskin, Lect. Math. Life Sci. **16**, 121 (1986).

[19] R. A. Simha and S. Ramaswamy, Phys. Rev. Lett. **89**, 058101 (2002).

[20] C. Dombrowski, L. Cisneros, S. Chatkaew, J. Kessler, and R. Goldstein, Phys. Rev. E **93**, 098103 (2004).

[21] D. Saintillan and M. J. Shelley, Phys. Rev. Lett. **100**, 178103 (2008).

[22] C. W. Wolgemuth, Biophys. J. **95**, 1564 (2008).

[23] M. Zajac and C. W. Wolgemuth, J. Comput. Phys. **229**, 7287 (2010).

[24] A. McMahon, W. Supatto, S. Fraser, and A. Stathopoulos, Science **322**, 1546 (2008).

[25] P. Friedl, Y. Hegerfeldt, and M. Tusch, Int. J. Dev. Biol. **48**, 441 (2004).

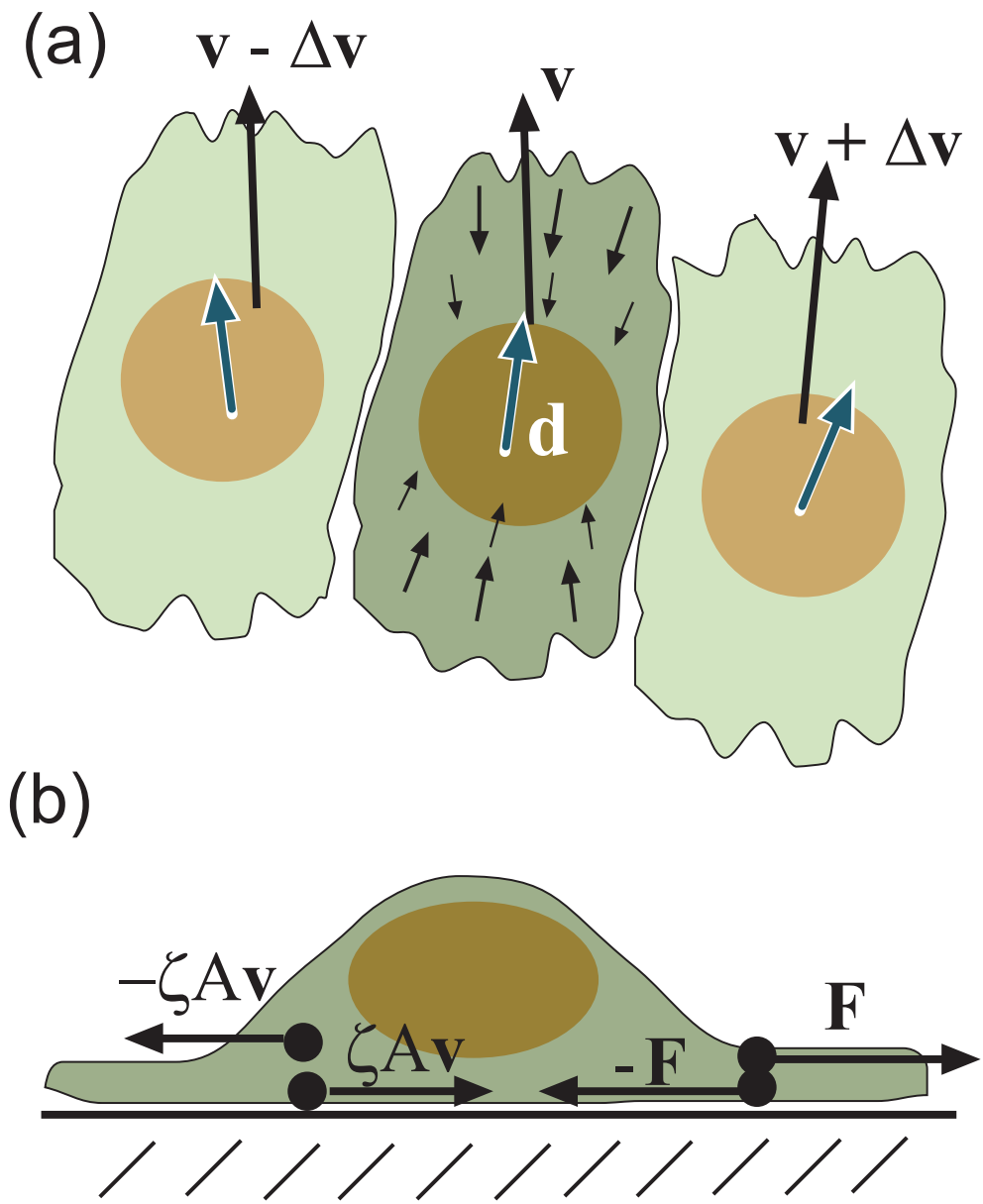

FIG. 1. (Color online) Schematic of the interactions affecting a cell crawling through a tissue. (A) A cell has a polarization direction, which is defined by the unit vector $\boldsymbol{d}$, and crawls with velocity $\boldsymbol{v}$. The cell exerts dipole-distributed forces against the substrate (small, black arrows). The cell is connected to its neighbors via adhesion proteins. Differences in velocity between the cell and its neighbors, therefore, lead to viscoelastic stresses in the tissue. (B) A single crawling cell exerts a thrust force $-\boldsymbol{F}$ on to the substrate. The substrate resists the motion of the cell with a force that is proportional to the velocity. Equal but opposite forces are exerted back on to the cell.

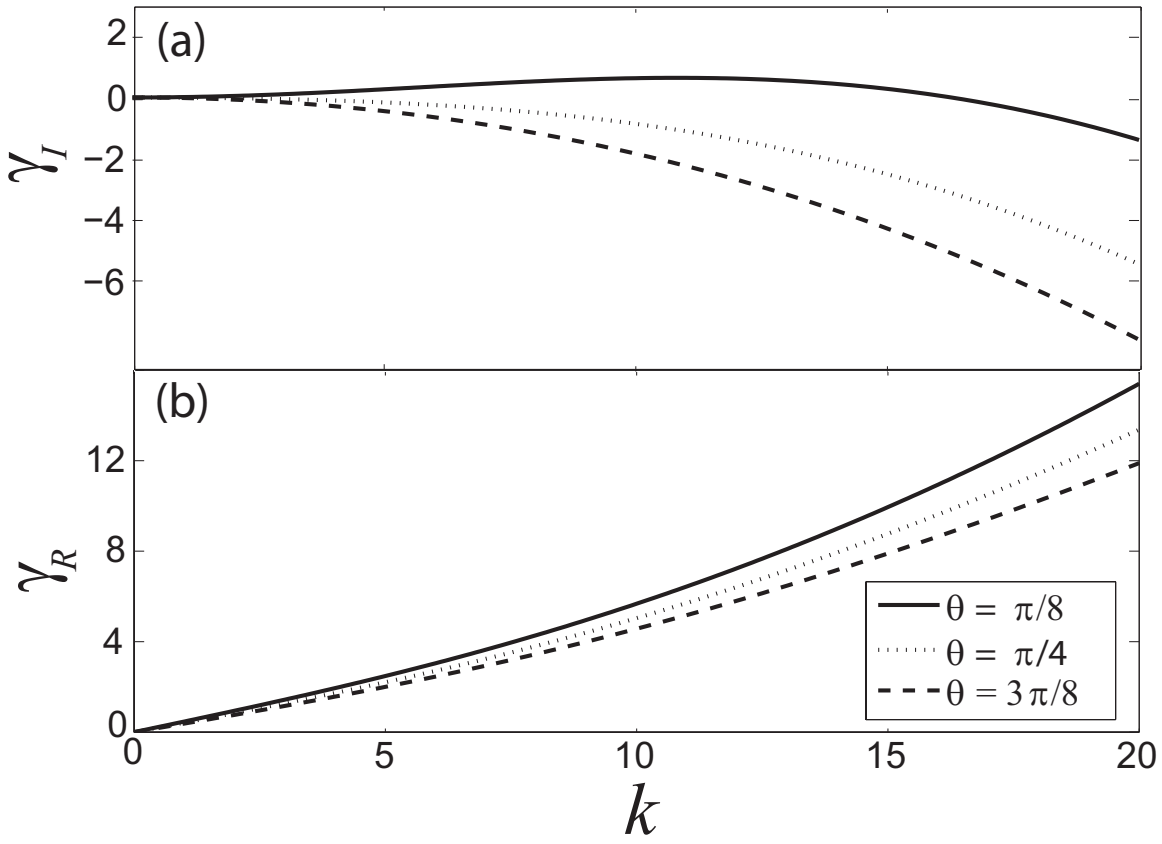

FIG. 2. The complex frequency as a function of the magnitude of the wavenumber $\boldsymbol{k}$ for $\theta = \pi/8$ (solid line), $\pi/4$ (dotted line), and $3\pi/8$ (dashed line). (a) The imaginary part of the frequency is the growth rate, which has a peak when $k = 10.8$. (b) The temporal frequency increases with wavenumber and is only weakly dependent on θ.

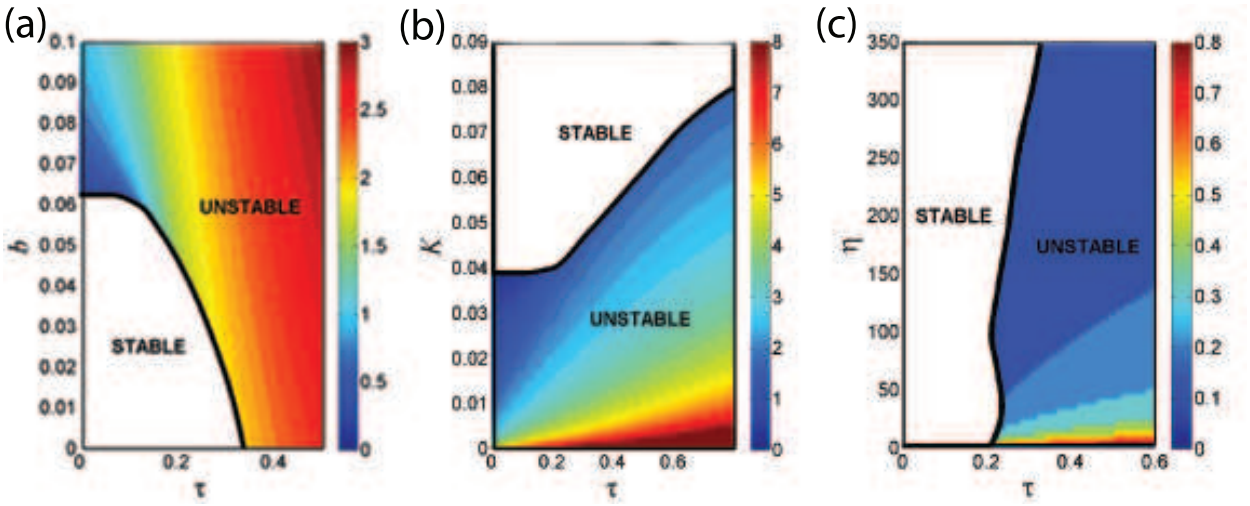

FIG. 3. (Color online) Two parameter bifurcation diagrams showing the regimes with stable, uniform cellular motion and those with complex cellular flows (unstable). Stability is shown as a function of (a) viscoelastic relaxation time τ and dipole stress strength b; (b) τ and orientational Franck constant K; and (c) τ and cell-cell viscosity η. The value of the other parameters are given above each panel. The colormap shows the magnitude of the wavenumber that corresponds to the maximally unstable mode.

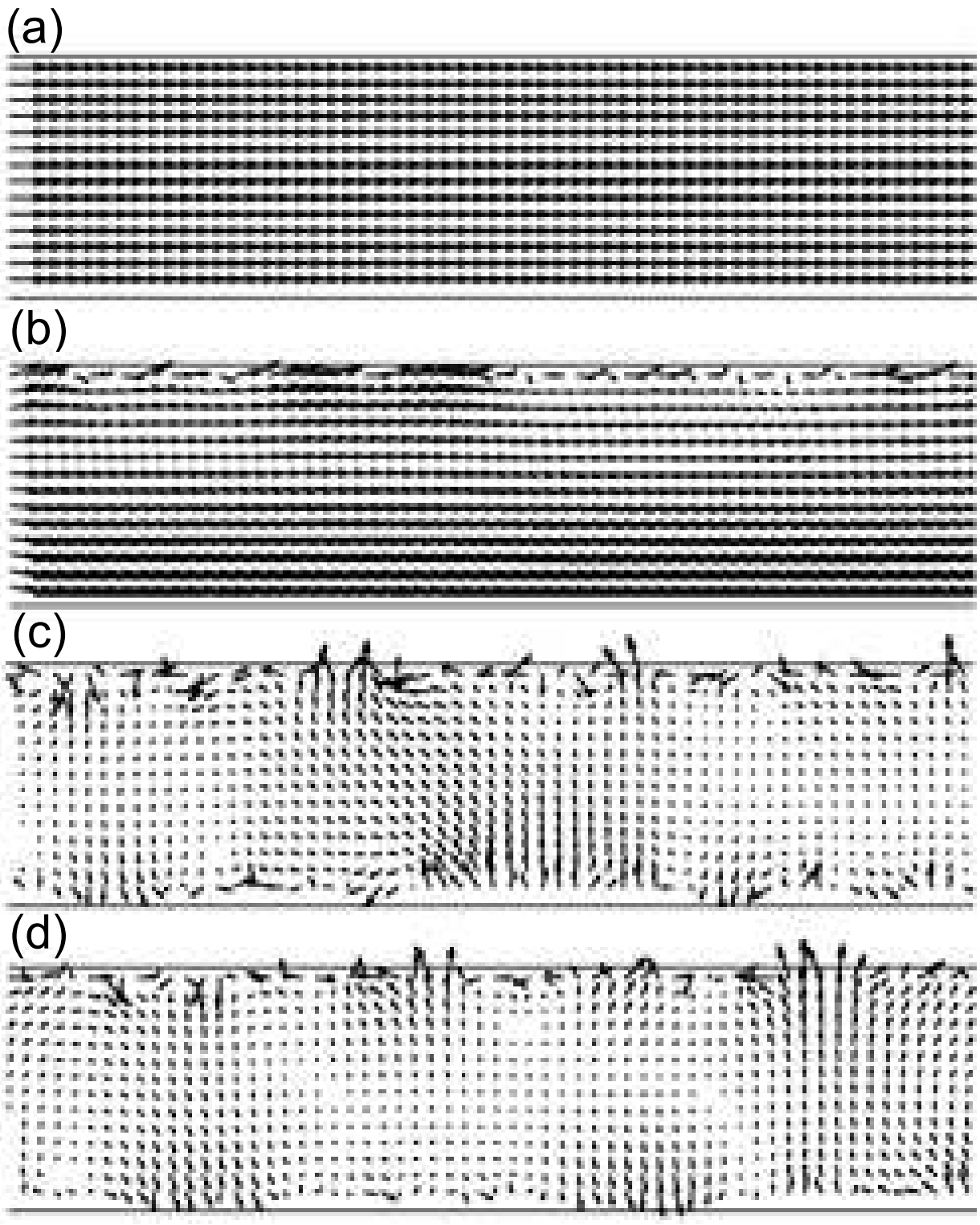

FIG. 4. Cellular flows of a confined epithelial layer: (a) Stable flow in the x direction. (b-d) Time series of the onset of the instability at $T = 0.03$, $T = 0.097$, and $T = 0.22$. Parameters used in the simulations are $b = 0.1$; $\eta = 0.0025$; $\lambda = 0.25$; $K = 0.0025$; and $\tau = 0.025$.